Materials and Structures (2023) 56:177
https://doi.org/10.1617/s11527-023-02265-y

ORIGINAL ARTICLE

Investigating the effect of hydrogel characteristics on the self-healing of cementitious materials

Babak Vafaei · Ali Ghahremaninezhad

Received: 23 January 2023 / Accepted: 14 October 2023 / Published online: 9 November 2023

Abstract Despite prior studies investigating the self-healing of cementitious materials containing hydrogels, the dependence of self-healing on the properties of hydrogels has not been sufficiently explored and is poorly understood. Thus, the novelty of this paper is to examine the self-healing of cementitious materials containing multiple hydrogels with different behaviors. Thermogravimetric analysis, Fourier transform infrared spectroscopy, and scanning electron microscopy equipped with energy dispersive x-ray spectroscopy were employed to probe the chemical characteristics of the healing products. The three-point bend test and optical microscopy were used to evaluate the mechanical strength recovery and crack filling, respectively, in the cementitious materials containing hydrogels. The healing products were shown to comprise calcium–silicate–hydrate (C–S–H), ettringite, calcium hydroxide, and calcium carbonate. The hydrogel modified paste with the highest water sorption demonstrated the highest calcium carbonate content. All hydrogel modified pastes exhibited improved strength recovery and crack filling compared to the control paste and this improvement was more pronounced in the paste with the highest water sorption.

B. Vafaei · A. Ghahremaninezhad (✉)
Department of Civil and Architectural Engineering, University of Miami, Coral Gables, FL 33146, USA
e-mail: a.ghahremani@miami.edu

Keywords Self-healing · Hydrogel · Healing products · Sorption · Cement paste

1 Introduction

Concrete is the most widely consumed material in the construction industry due to its desirable properties, wide availability, low cost, and ease of manufacture. However, concrete suffers from low tensile strength making it susceptible to cracking when subjected to mechanical and environmental stressors [1, 2]. When cracks develop in concrete, they provide preferential access for harmful substances (e.g., chlorides, sulfates, and carbonates) to penetrate the material, which causes the corrosion of reinforcement steel and other degradation processes [3]. Thus, cracking severely compromises the service life of concrete structures. The manual repair and maintenance of concrete structures are costly and labor-intensive, and these costs are expected to rise as structures age. Approximately, 27% of all highway bridges in the USA need repair, and the corrosion related deterioration costs have been estimated at over 150 billion dollars [4]. Furthermore, not all parts of structures are accessible for damage monitoring and maintenance. Therefore, using self-healing materials could be a viable method to tackle the cracking issues in concrete structures.

Cementitious materials have an intrinsic self-healing capability via the autogenous healing mechanisms [5]. As revealed in previous studies, the main forms of autogenous healing in cementitious materials can be summarized as further hydration of unreacted cement particles, pozzolanic activity, and precipitation of calcium carbonate [6–11]. Since there are always some unreacted cement particles in the material, when water penetrates through the cracks and comes in contact with these unreacted cement particles, further hydration of the unreacted particles occurs, which could lead to the healing of the crack. Moreover, if water and carbon dioxide are present near the crack surfaces, another mechanism of self-healing, precipitation of calcium carbonate, takes place [12, 13]. While both of these mechanisms could progress concurrently, continued hydration seems to be dominant at early ages, and calcium carbonate precipitation occurs more prevalently at later ages [14]. The presence of water is an essential part of the self-healing mechanisms; however, this is not always the case in practical conditions. A potential solution to overcome this issue is incorporating superabsorbent polymers (SAPs) or hydrogels into concrete [14–17]. Hydrogels are able to absorb and retain fluids and moisture from the surrounding environment and provide water to promote the autogenous healing mechanisms by gradually releasing it into their surroundings during dry periods [12, 18]. The efficiency of hydrogels as an internal curing agent and their effects on autogenous shrinkage, mechanical properties, hydration, and microstructure of Portland cement binders [19–26] and alkali-activated slag binders [27–31] have been studied in the past. The improved self-healing in cementitious materials with hydrogels up to the ages of 8 years [32] and 10 years [33] was indicated in the previous studies. Previous studies examined the effect of hydrogels on the filling and crack closure of cementitious materials using optical microscopy [34, 35], x-ray microcomputed tomography [36], and nuclear magnetic resonance (NMR) [37]. The sealing and water tightness of the healed cementitious materials with hydrogels were assessed using the permeability measurements [38, 39]. The self-healing performance was also evaluated using the mechanical testing [14, 17, 34, 40, 41] and recently ultrasonic mapping [35]. The chemical attributes of the healing materials were examined in a few prior investigations [1, 42–44]. While there have been several studies on the self-healing of cementitious materials containing hydrogels, the link between hydrogel characteristics and their self-healing performance is poorly understood. The novelty of this research is to contribute to our understanding of the hydrogel characteristics—self-healing property relationships in cementitious materials. Such an understanding is needed to inform design guidelines for self-healing cement-hydrogel systems. To this end, this paper examines the effect of hydrogels with different chemical compositions and absorption behaviors on (1) the phase composition and microstructure of healing products and (2) the mechanical recovery and crack closure of cementitious materials. Thermogravimetric analysis (TGA), Fourier transform infrared spectroscopy (FTIR), and scanning electron microscopy equipped with energy dispersive x-ray spectroscopy (SEM/EDS) were used for material characterization. The three-point bend test was conducted to assess the mechanical recovery of prisms. Crack closure was monitored using optical microscopy.

2 Experiments

2.1 Materials

2.1.1 Hydrogels

Hydrogels used in the concrete applications are primarily comprised of a crosslinked copolymer of acrylamide and salt of acrylic acid. In this study, four hydrogels with different chemical compositions were synthesized and used in the experiments. The chemical compositions of the hydrogels and their designations are listed in Table 1. All chemicals utilized in synthesizing the hydrogels were purchased from Sigma-Aldrich. The synthesis was carried out using the free radical polymerization method [25, 45–50]. First, acrylic acid monomers (AA) were dissolved in 100 mL of distilled water, followed by partial neutralization of AA by sodium hydroxide (NaOH). Then, acrylamide monomers (AM) and 0.05 g of the crosslinking agent, *N*,*N*′-methylenebisacrylamide (MBA), were added to the solution. The solution was stirred for 30 min to ensure complete dissolution. Then, the solution was sparged with argon gas for 3–5 min to remove entrapped gasses. The

Table 1 Compositions of the hydrogels synthesized in the experiment

Hydrogel	Distilled water (g)	AA (g)	AM (g)	NaOH (g)	MBA (g)	APS (g)	Nanosilica powder (g)	Colloidal nanosilica (g)
H-a	100	10	10	1.35	0.05	0.128	–	–
H-b	100	2	18	0.27	0.05	0.128	–	–
H-c	100	–	20	–	0.05	0.64	10	–
H-d	50	–	20	–	0.05	0.64	–	50

polymerization initiator, ammonium persulfate (APS), was added to the solution in the amount of 0.128 g. The main monomers in H-a and H-b were AA and AM with different concentrations; AA and NaOH were not used in synthesizing H-c and H-d; instead, nanosilica in the form of a powder and colloidal nanoparticles were used. The reason for using nanosilica was to achieve different absorption characteristics in the hydrogels. The solutions, prepared in glass containers, were then placed in the oven at 50 °C for 3 h to allow gelation to occur. Then, all hydrogels were demolded and broken into small pieces. H-a and H-b were submerged in distilled water for 24 h to remove unreacted monomers. H-c and H-d were not submerged in distilled water to eliminate the possibility of nanosilica particle leaching out of the hydrogels. However, our later examination did not show any evidence of leaching. Then, the hydrogels were washed and dried in an oven at a temperature of 60 °C for 1 week. When fully dried, the hydrogels were ground using a coffee grinder and sieved using a shaker (RX-29, WS TYLER). The hydrogel particles in the size range of 75–300 μm were used in the experiments. The hydrogels were sealed in polyethylene bags and stored in a desiccator to prevent moisture uptake. Figure 1 shows the images of the hydrogel synthesis and the SEM images of all hydrogel particles. It is noted that the hydrogel particles had an angular shape.

2.1.2 Cement mix design

A type I/II Portland cement manufactured by CEMEX with a minimum 28-day compressive strength of 28 MPa was used in producing the pastes. Table 2 shows the chemical composition of the cement as provided by the manufacturer. A ZYLA water-reducing admixture manufactured by GCP incorporating highly purified specialty organic matter was used to improve the flowability of the mixtures. Table 3 presents the mix designs of the cement pastes used in the experiments. The control paste is designated as C; C H-a, C H-b, C H-c, and C H-d refer to the paste with H-a, H-b, H-c, and H-d, respectively. Control paste without hydrogels with a water/cement (w/c) of 0.3 was prepared. The flow of the control paste was measured to be 20 cm using a flow table test. The pastes with hydrogels were prepared with a hydrogel concentration of 1% per cement mass and with the same effective (w/c) of 0.3 as the control paste. This concentration of hydrogel was reported to be efficient for self-sealing and self-healing [51–53]. In order to account for the absorbed water in the hydrogels, additional water was added in increments to the pastes with hydrogels until the same flow value of 20 cm was achieved in all pastes. The flow test method is detailed in our previous studies [19, 22, 27]. In this test, pastes were poured into a cone (height = 50 mm; bottom diameter = 70 mm; top diameter = 100 mm), and allowed to rest on a table for 5 min. Then, the cone was removed, and the table was dropped 25 times in 15 s with a consistent frequency. The average of the two perpendicular bottom diameters of the pastes was measured. The flow test was performed three times and the average value was reported. Dry hydrogel powders were first dry mixed with cement for 5 min. A ZYLA water-reducing admixture at a concentration of 0.17% per cement mass was used in all mixtures. Then, after the initial contact of the cement and dry hydrogel mix with water for 30 s, the mixture was mixed at a speed of 440 rpm for another 30 s. After scraping the inside wall of the container for 15 s, the

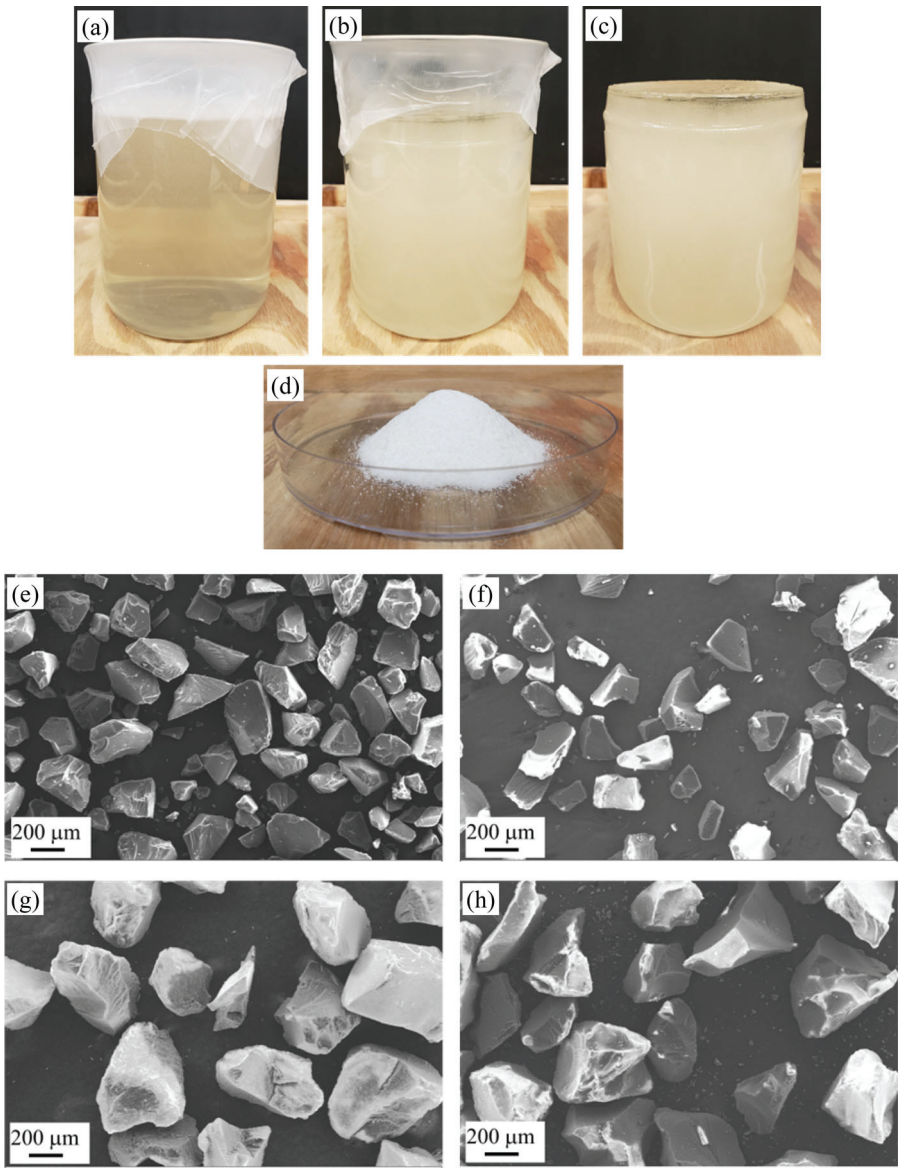

Fig. 1 Images of the hydrogel synthesis corresponding to **a** before gelation, **b** after gelation, **c** after being demolded, and **d** after being ground to powder. SEM images of **e** H-a, (f) H-b, **g** H-c, and **h** H-d. SEM parameters are: Voltage = 25 kV, Magnification = 50X, and Working distance = 10 mm

mixing continued at a higher speed of 2600 rpm for 60 s. The pastes were then poured into cubic molds of dimensions 50 mm × 50 mm × 50 mm. The pastes were poured in two layers and each layer was tamped according to ASTM C 109. The molds were wrapped with a pre-stretch plastic foil and stored in double-layer polyethylene bags to prevent water evaporation. After demolding, the cementitious cubes were stored in double-layer bags until testing.

2.2 Methods

2.2.1 Re-absorption of hydrogels

As discussed previously, the supply of water from hydrogels into their surrounding area on the crack surface is an important factor underlying the self-healing ability of hydrogels. Due to the chemical interactions between the hydrogels and the cement

pore solution, including Ca^{2+} complexation, the subsequent absorption behaviors of hydrogels could be affected compared to the virgin hydrogels. Thus, in order to gain insights into such effects, the re-absorption of the hydrogels after being subjected to an extracted pore solution was measured using the teabag test [54]. Recommendations for measuring hydrogel absorption has been discussed in the literature [55]. To this end, the extracted pore solution of a cement mixture with a w/c of 1 was obtained using centrifugation at 4400 rpm for 5 min. Approximately 0.2 g of hydrogels were placed in a teabag and submerged in 500 mL of extracted pore solution for 80 min. For each hydrogel, 5 replicates were used. Then, the swollen hydrogels were removed from the teabags, placed in petri dishes, and dried in a vacuum oven at a temperature of 60 °C for about 20 days. The hydrogel mass was monitored to ensure a constant mass was achieved in the dried hydrogels. For mass measurements, the hydrogels were taken out of the vacuum oven for a short period of time. Then, the hydrogels were crushed, sieved to a size range of 75–425 mm, and stored in sealed glass vials. The dried hydrogels were poured into new teabags and re-submerged into the extracted pore solution. At specific time intervals, the teabags were removed from the solution, gently surface dried and their mass recorded. To account for the water absorbed by the teabag, the mass of 5 empty teabags removed from the solution was averaged and recorded. The re-absorption of the hydrogels was measured using the following equation:

$$\text{Re-absorption} = \frac{X_{wh} - X_w - X_h}{X_h} \quad (1)$$

where X_h, X_w, and X_{wh} are the mass of dry hydrogel, wet teabag without hydrogel, and wet teabag with hydrogel, respectively.

Table 2 Oxide composition of the cement

Composition	(%)
SiO_2	20.6
Al_2O_3	4.8
Fe_2O_3	3.5
CaO	64
MgO	0.9
Na_2O	0.1
K_2O	0.3
SO_3	3.4

2.2.2 *Healing products characterization*

2.2.2.1 Sample preparation In order to overcome the difficulty of separating the healing products from the cementitious matrix, instead of real cracks, artificial planar gaps were created as utilized in a prior study [56]. To this end, cement paste cubes at the age of 7 days were dry sliced into the dimensions of 50 mm × 50 mm × 15 mm, and their cut surface polished with sandpapers of grit sizes 320, 500, and 1200, followed by a 1 μm diamond paste abrasive. Water was used as the lubricating liquid during polishing with sandpapers. After polishing, the slices were dried in a vacuum oven. The cement paste slices were then pressed together and healed in the water for 14 days. Figure 2 shows the details of the setup used for studying the healing products. The gap between the slices was measured to be about 40 mm using an optical microscope. With this setup, the healing products can be easily scratched off from the slice surfaces using a razor blade. Only about 4 mm from the bottom of the slices was submerged in water, and the water was transported into the gaps due to the capillary force. The healing products were dried in a

Table 3 Mix designs and the flow values of the cement pastes, and hydrogel absorption

Paste designation	Water/cement	Water-reducing admixture (% per cement mass)	Hydrogel (% per cement mass)	Flow (cm)	Hydrogel	Absorption from the flow test (% g/g)
C	0.3	0.17	–	20	–	–
C H-a	0.45	0.17	1	20	H-a	1500
C H-b	0.55	0.17	1	20	H-b	2500
C H-c	0.38	0.17	1	20	H-c	800
C H-d	0.42	0.17	1	20	H-d	1200

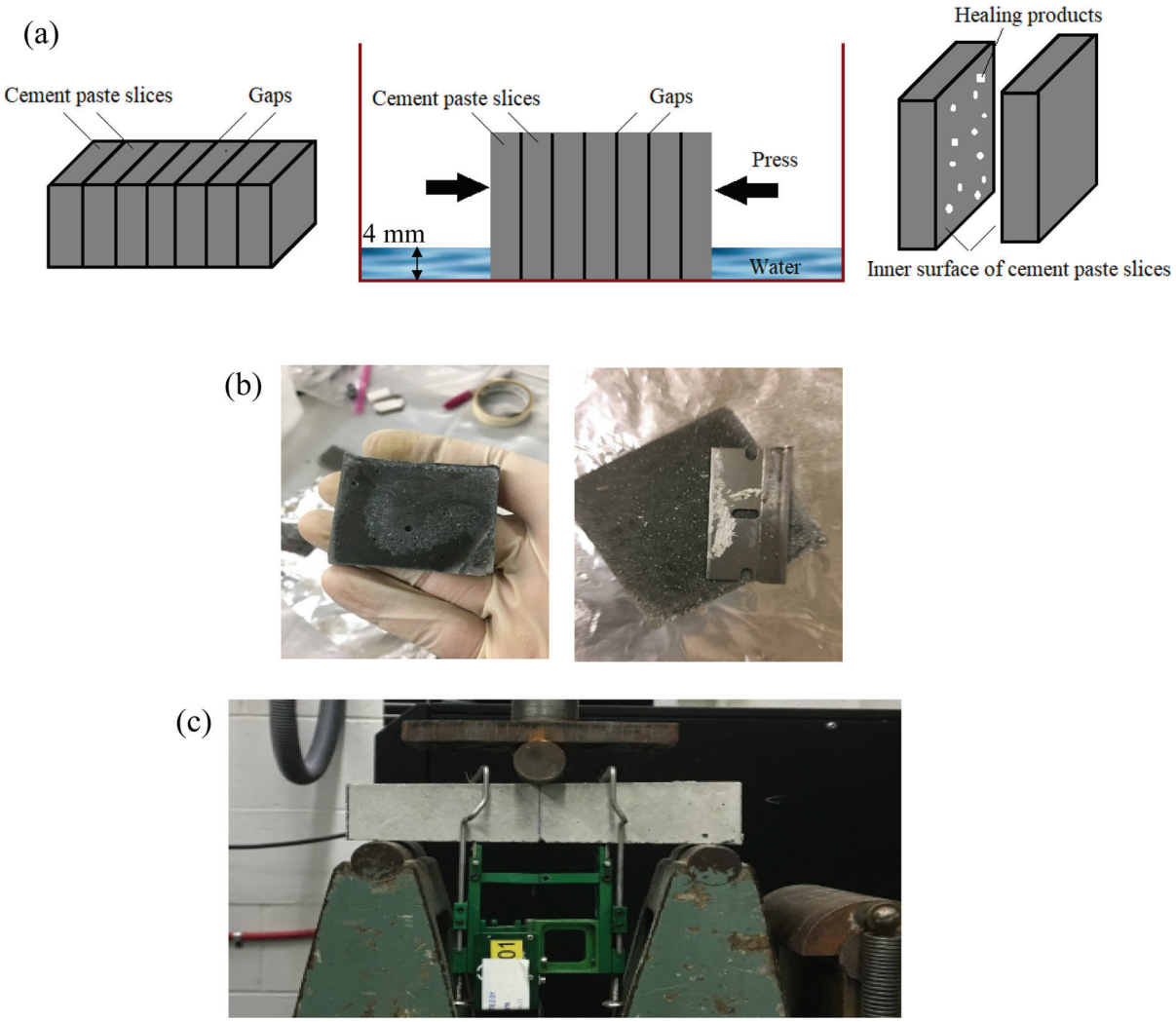

Fig. 2 **a** Schematic of sample preparation for the chemical characterization of the healing products. **b** Images showing the formation of healing products in the gap between the cement paste slices. **c** Three-point bend setup used in the strength recovery measurements of the pre-cracked cement paste prisms

vacuum oven at a temperature of 40 °C for 24 h and then used in TGA, FTIR, and SEM/EDS. The healing products formed on the surface before being scratched off were imaged using a KEYENCE VHX 5000 digital microscope.

2.2.2.2 Sorption This test was performed to determine the water absorption via the capillary suction, i.e., sorption, through the gaps in the cement paste slices by measuring the increase in the sample mass as a function of time. Cement slices were first dried in an oven for 1 week at a temperature of 60 °C. Then, the top and four sides of the samples were sealed using an aluminum tape to allow capillary suction from only the bottom side in contact with water. After measuring the dry mass of the samples, they were partially placed in distilled water with a submerged depth of 4 mm, and their mass was measured at certain time intervals in the first day and every day for the next 14 days. Before every measurement, the bottom of the samples was surface dried using a paper towel. The sorption was then determined using the following equation:

$$\text{Sorption} = \frac{M_{\text{wet},t} - M_{\text{dry}}}{M_{\text{dry}}} \quad (2)$$

where $M_{wet,t}$ is the mass of the sample at time t and M_{dry} is the dry mass of the sample before exposure to water.

2.2.2.3 TGA Approximately 30–40 mg of the healing products was used in TGA. The samples were analyzed at a heating rate of 10 °C/min and in the temperature range of 23–1000 °C in a TGA 55 TA Instrument under nitrogen gas. The normalized contents of calcium hydroxide (CH) and calcium carbonate (CC) were determined by Eqs. 3 and 4, respectively:

$$\mathrm{CH} = \frac{74.1}{18}\frac{\overline{M}}{M} \tag{3}$$

$$\mathrm{CC} = \frac{100}{44}\frac{\overline{M}}{M} \tag{4}$$

where $\overline{M}$ (mg) is the mass change corresponding to the decomposition of CH and CC, respectively, and M (mg) is the initial sample mass.

2.2.2.4 FTIR FTIR was performed on the healing products using a Perkin Elmer Paragon 1000 FTIR with an ATR accessory in the transmission mode in the range of 600–4000 cm^{-1} and at the resolution of 4 cm^{-1}.

2.2.2.5 SEM/EDS The morphology of the healing products was observed using a JEOL SEM equipped with EDS. Since electrical conductivity is critical for imaging quality, the samples were gold coated using a sputter coater. Images were taken at the acceleration voltage of 15 kV and the magnification of 50 Kx. Elements were analyzed by selecting random points on the surface of the healing products using EDS.

2.2.3 Strength recovery and crack closure experiments

The effect of the different hydrogels on the strength recovery and crack closure of the cementitious materials was examined in this section. Paste prisms of dimensions 2.54 cm × 2.54 cm × 15 cm and with the same mix designs as detailed in Table 3 were cast. All prisms were notched at their center using a rotating diamond blade. The notch width and depth were 2.0 and 1.5 mm, respectively. In order to generate cracks in the prisms, the prisms were loaded in a three-point bend setup (see Fig. 2c) at a rate of 0.0002 mm/s using an Instron testing machine. 38 μm diameter PVA fibers at a volume percentage of 2% were added to the paste prisms to increase ductility and prevent complete failure during initial crack generation. The crack opening was monitored using a clip gage. The loading was stopped when the crack opening reached 0.2 mm, and then the prisms were unloaded. The crack width after load removal was measured for all prisms using the optical microscopy and was about 60 ± 8 μm. The cracked samples were then subjected to dry/wet cycles at the room temperature of 23 °C for 28 days in standard laboratory conditions. A dry/wet cycle included 1 h of wet period, where the prisms were submerged in water, and 23 h of exposure to the atmosphere with relative humidity (RH) of 60 ± 5%. The volumetric ratio of the water to the prisms during the wet cycle was 5. After 28 days (28 cycles), the prisms were loaded until failure in the three-point bend setup. The strength recovery (SR) was calculated as follows:

$$\mathrm{SR}(\%) = \frac{P_{max,healing} - P_{unloading}}{P_{max,initial} - P_{unloading}} \times 100 \tag{5}$$

where $P_{max,initial}$ is the maximum load achieved during the first loading to generate initial crack width, $P_{max,healing}$ is the maximum load attained by the healed prisms, $P_{unloading}$ is the residual load, which corresponds to the load at which the initial predefined crack width was reached followed by unloading. To monitor crack closure in the prisms, the cracks on both sides of the prisms were imaged after 1, 3, 7, 14, and 28 cycles of healing using a KEYENCE VHX 5000 digital microscope.

3 Results and discussion

3.1 Absorption results using the flow test

The absorption of the hydrogels in cement paste obtained from the flow test is listed in Table 3. It is seen that H-b showed notably higher absorption compared to other hydrogels. The order of hydrogel absorption is as follows: H-b > H-a > H-d > H-c. In cement pore solution, several ions including K^+, Na^+, Ca^{2+}, and OH^- are released into the solution as

cement particles hydrate. These ions can affect the absorption of hydrogels via the screening effect and Ca^{2+} complex formation as evidenced in the previous studies [47, 57, 58]. The reason for the higher absorption of H-b compared to H-a is due to a lower concentration of AA in the molecular structure of H-b compared to H-a as indicated in Table 1; it is known that hydrogels with a higher concentration of negatively charged AA are more susceptible to the screening effect and complex formation with Ca^{2+} in the cement paste environment [47, 57, 58]. The lower absorption of H-c and H-d, compared to H-b is due to a higher concentration of polymeric constituents (100%) in H-b; H-c and H-d had nanosilica in different concentrations in their composition, which does not contribute to water absorption of the hydrogels. As indicated previously, the reason for preparing hydrogels with nanosilica was to obtain hydrogels with different absorption behaviors and examine their effect on the healing processes.

3.2 Re-absorption of hydrogels

The results of the re-absorption test of the hydrogels are depicted in Fig. 3. The re-absorption of the hydrogels was measured after the hydrogels had been subjected to extracted pore solution and dried, as explained previously. It is noted that all hydrogels showed a retentive behavior and were able to retain the absorbed fluid during the test [59]. It is noted that the re-absorption of the hydrogels is lower than their absorption, which is due to the change in the ionic composition and formation of irreversible complexes between Ca^{2+} and the polymeric network of the hydrogels. Nonetheless, it is seen that the re-absorption trend of the hydrogels was generally similar to their absorption trend as obtained from the flow test. H-b demonstrated the highest re-absorption, followed by H-a, H-c, and H-d. It is noted that H-c showed a slightly higher re-absorption compared to H-d, which could be due to the difference in the water availability in the flow test compared to the teabag test; the flow test was conducted in cement paste while the teabag test was carried out in a solution.

3.3 Sorption of cement paste slices

The sorption of the cement paste slices with and without different hydrogels is shown in Fig. 4. It is seen that C H-b showed the highest water sorption and the control paste, C, had the lowest water sorption. C H-a and C H-d had a similar sorption behavior, and the sorption of C H-c was lowest among hydrogel-modified cement pastes. Interestingly, the water sorption of the pastes generally followed a similar trend to the water re-absorption results shown in Fig. 3. The sorption of cementitious materials is governed by the capillary forces due to the presence of fine capillary pores in the microstructure of the cement pastes. The sorption of cement paste slices is related to the overall water/cement of the pastes. The relationship between the sorption and water/cement of cementitious materials has been extensively studied in the past [60] where an increase in the water/cement was shown to result in higher capillary porosity. The cement pastes used in our study had the same effective

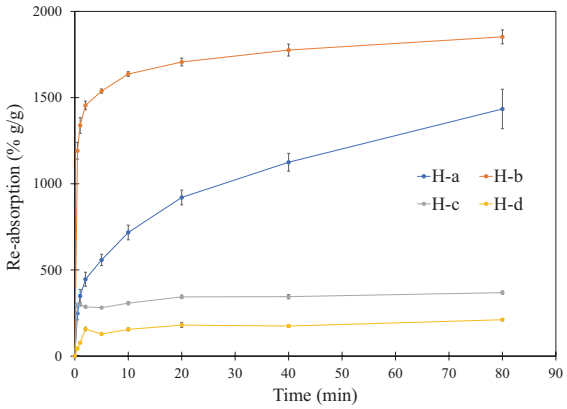

Fig. 3 Re-absorption of the different hydrogels in an extracted pore solution

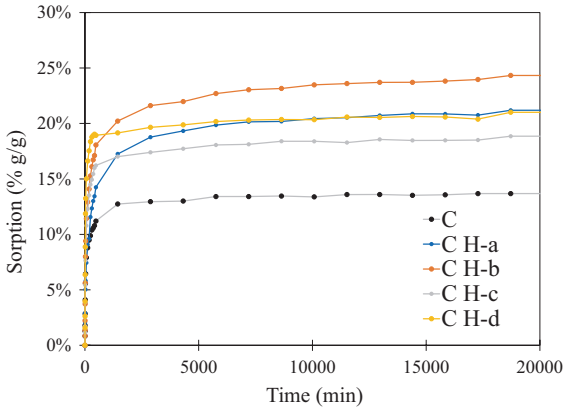

Fig. 4 Sorption of the cement paste slices without and with hydrogels

water/cement of 0.3; however, the overall water/cement was different due to the difference in the water absorption of the various hydrogels used in their mix design. Thus, the observed sorption of the cement paste slices was to be expected. It should be noted that the re-absorption of the hydrogels could have a potential influence on the sorption results as the hydrogels could serve as a water reservoir; however, it is difficult to estimate the actual re-absorption of hydrogels in the cement pastes and decouple that from the capillary-driven water sorption. Since the presence of water and Ca^{2+} leaching are important factors in the formation of healing products in the gap between the cement paste slices, the above-mentioned results could provide useful insights into understanding the underlying mechanisms.

3.4 Optical microscopy of healing products

Figure 5 demonstrates an optical image of representative healing products corresponding to C. Healing products are seen as a whitish feature and the cement paste surface as a dark greyish feature in the image. It is seen that the healing products had a porous morphology and did not seem to have a uniform coverage over the gap surface at the microscale. While C H-b exhibited more healing products compared to the sample with other hydrogels, the optical imaging of all samples showed similar features.

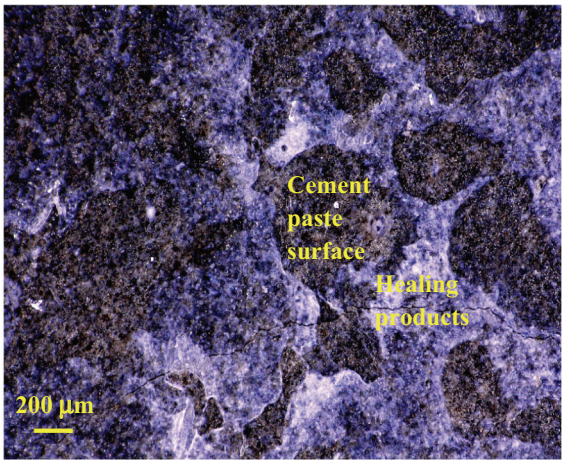

Fig. 5 Optical image showing healing products formed on the surface of C. The healing products are seen as a whitish feature and the cement paste surface as a dark greyish feature in the image

3.5 TG/DTG of healing products

Figure 6a and b show the TG and DTG curves, respectively, of the healing products (HP) as well as the corresponding bulk pastes at the age of 7 days. Similar to the TG and DTG curves of the bulk cement pastes, three significant peaks can be identified in the TG curves of healing products scratched off from the surfaces of planner gaps. The mass loss at the temperature between 70 and 200 °C is attributed to the evaporation of free water and dehydration of C–S–H and ettringite [61–63]. Nevertheless, it is difficult to distinguish between these phases by TG/DTG, since they are generally decomposed between 70 and 200 °C [64, 65]. It is noted that these peaks are weaker in the case of healing products compared to the bulk pastes. A mass loss was observed at the temperature between 400 and 550 °C. This mass loss is attributed to the decomposition of calcium hydroxide [19, 66–68]. The sample weight decreases further

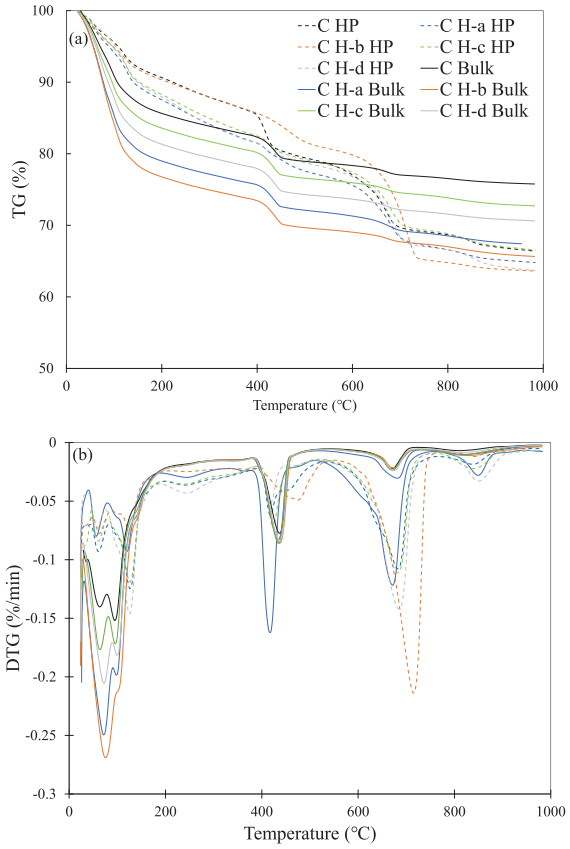

Fig. 6 **a** TG and **b** DTG curves of the healing products (HP) and bulk of the cement pastes with and without hydrogels

when the temperature rises from 550 to 750 °C, which is caused by the decomposition of calcium carbonate [66, 69–72]. A slight mass loss is visible in the temperature range of 800–900 °C, which may be related to the decomposition of calcium carbonate [73, 74]. This peak appears to be more pronounced in the case of healing products than the bulk cement paste.

The CH and CC contents of the healing products and bulk pastes are shown in Fig. 7. A major observation is a higher CH content and more noticeably higher CC content of the healing products compared to the bulk paste. The C-S–H resulting from the hydration of unhydrated cement particles on the surface of the crack (slice surface) forms in the region immediately surrounding the unhydrated cement particle [75, 76]. On the other hand, CH and subsequently CC, tend to form in large spaces, so cracks are favored sites for CH and CC precipitation [76]. In addition, the concentration of Ca^{2+} in the solution in the crack is less than that in the bulk; thus, Ca^{2+} and other ions can leach from bulk into the crack, increasing ionic concentration, when the supersaturation conditions are reached, CH and CC, provided dissolved CO_2 is present, are formed. It should be noted that the diffusion of silicate ions is smaller than Ca^{2+} [77]. The above-mentioned processes explain the higher content of CH and CC in the healing products compared to the bulk paste.

It is noted from Fig. 7 that the CC content of the healing products in the paste with hydrogel is generally higher than that of the control paste, and this was more pronounced in the case of C H-b. On the other hand, the CH content followed an opposite trend compared to the CC content. This could indicate that the higher supply of water from the hydrogel on the crack surface, in conjunction with the available dissolved CO_2, favors the precipitation of CC over CH. It is interesting to note that the increase in CC content seemed to generally follow the sorption of the paste slices, as shown in Fig. 4. The relationship between CC content and the sorption of the pastes can be explained in light of the fact that water is needed for the carbonation reaction and also it facilitates the transport of Ca^{2+} from the interior bulk to the crack space.

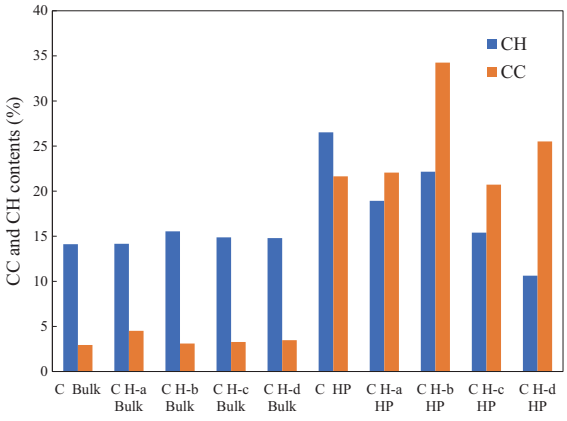

Fig. 7 CC and CH contents of the healing products and bulk of the pastes with and without hydrogels

3.6 FTIR of healing products

The FTIR analysis was carried out to obtain information on the mineralogy of the healing products. Figure 8 shows the FTIR spectra of the cement clinker, bulk control cement paste, and healing products corresponding to C H-a, C H-b, C H-c, and C H-d. All these spectra demonstrated a complex group of bands in the range of 800–1200 cm^{-1}, related to the stretching vibration of Si–O bonds [78]. Due to the hydration of the cement paste, the main band in the spectrum of the cement clinker at 877 cm^{-1} shifted to the 967 cm^{-1} and 1110 cm^{-1} in the profile of the bulk cement paste and healing products, which is attributed to the Si–O stretching vibrations in C–S–H gels [22, 79–82]. It is to be noted that the S–O stretching peak of SO_4^{-2} also has a peak at 1110 cm^{-1}, which could indicate the presence of ettringite. The small band at 3640 cm^{-1} occurred in the spectrum of the bulk cement paste and the healing products and is attributed to the formation of calcium hydroxide [79]. The C–O bending vibration at about 874 cm^{-1} and the bands in the range of 1400–1500 cm^{-1} are observed in the spectra of the healing products only and are the characteristic band of CO_3^{2-} [79, 80], that can be attributed to the presence of calcium carbonate. This observation agrees with the significantly higher CC content in the healing products, as noted in the TGA analysis shown in Fig. 7. The broad band at about 3400 cm^{-1} is attributed to stretching vibrations of O–H groups in water [79]. The peak at about 1640–1650 cm^{-1} is also attributed to the bending vibration (O–H) in water. The peak at 3640 cm^{-1}

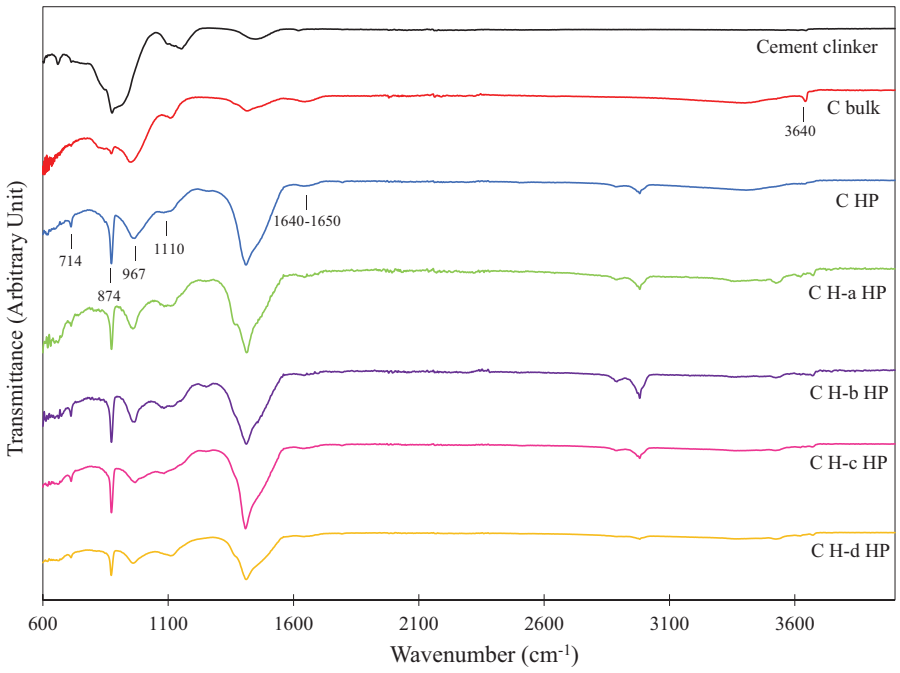

Fig. 8 FTIR spectra of the bulk cement paste and the healing products corresponding to the cement paste slices with and without hydrogels

confirmed the presence of calcium hydroxide in the healing products which was observed in the TGA and DTG profiles [56]. A peak at approximately 2985 cm^{-1} corresponds to the stretching vibration of the carbon-hydrogen (C–H) group in organic matters, which could be derived from the superplasticizer used in the mixtures.

3.7 SEM/EDS of the healing products

The morphology of the healing products formed on slice surfaces was observed using SEM, as illustrated in Fig. 9a. Different morphologies can be observed in the healing products. The needle-like morphology appears to be present sporadically and is attributed to ettringite [83]. Plate-like crystals are seen in the morphology of the healing products, which resemble $Ca(OH)_2$. The planar size of the plate-like crystals is in the range of a few micrometers. A gel-like morphology is noted, which is most likely C–S–H gel [84]. Moreover, there exist rhombohedral calcite crystals in the morphology of the healing products. This is in agreement with the TGA and FTIR results that indicated the presence of CH, C–S–H, ettringite, and $CaCO_3$ in the profiles of the healing products. The SEM examination did not reveal noticeable differences between samples with different hydrogels indicating that the healing products consisted of similar phases. Thus, the addition of hydrogels affected the composition of the healing products; however, new phases did not form in the healing products.

The chemical elements of the healing products of the control paste and pastes containing hydrogels were investigated using EDS. The EDS results showed that calcium, silicon, aluminum, potassium, sulfur, iron, carbon and oxygen were present in the healing products. The EDS confirmed the presence of sulfur in the healing products, which could be attributed to the ettringite.

The Ca/Si and Al/Si of the healing products as well as the bulk paste are shown in Fig. 10. The Ca/Si and Al/Si of the healing products are higher than those of the bulk cement paste. It should be noted that the X-ray data in the EDS comes from an area below the surface. The emission penetration depth of the X-ray is dependent on the applied acceleration voltages and the atomic number of the elements. According to [56, 85], the penetration depths range from 3 to 5 μm, when the applied acceleration voltage is 15 kV. Thus, there is a possibility that other elements surrounding the objective phase are detected by EDS. An explanation for higher Ca/Si and Al/Si of the healing products is related to the diffusivity of the phases and

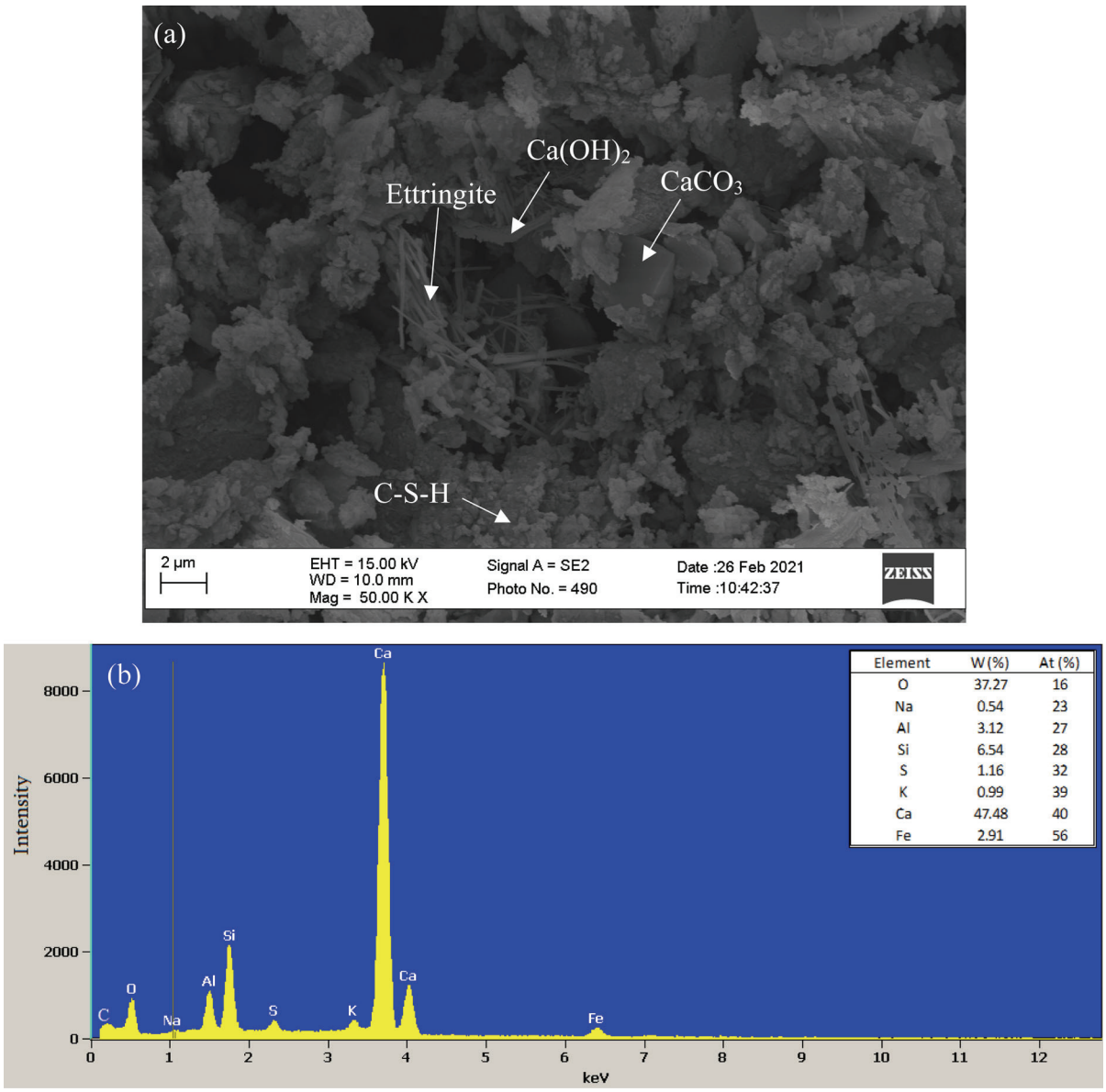

Fig. 9 **a** SEM image showing the morphology of the microstructure and **b** EDS spectrum of the healing products corresponding to C Paste

elements in the bulk cement paste. According to [76, 86], C–S–H tends to precipitate surrounding the cement particles. During the hydration of unhydrated cement, the majority of Si is consumed to produce the inner products, which occupies the original space of unhydrated cement. In other words, it is more difficult for Si ions to diffuse far away from unhydrated cement, compared to Ca^{2+} and Al^{3+} ions [56, 77]. Therefore, less Si can be found in healing products, leading to a relatively higher Ca/Si and Al/Si in the healing products than in the bulk cement paste matrix. Regarding the effect of the hydrogels on the elemental composition of the healing products, there appears to be a slight increase in Ca/Si in the sample with hydrogels compared to the control sample (C HP). However, no relationship between Ca/Si and the hydrogel characteristics can be established due to a large scatter in the results.

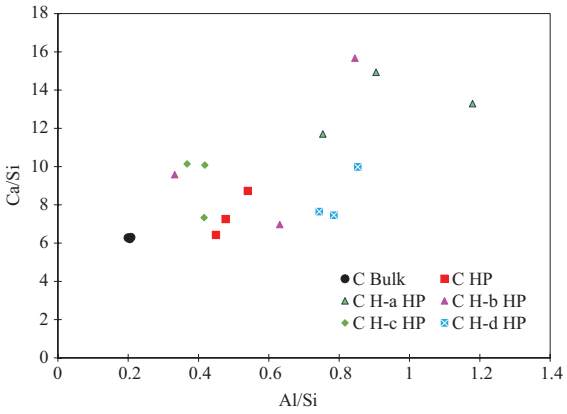

Fig. 10 Ca/Si and Al/Si of the healing products (HP)

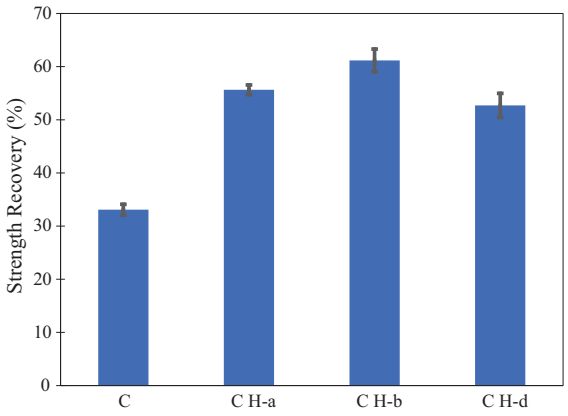

Fig. 11 Strength recovery of the prisms with and without different hydrogels

3.8 Regain in mechanical properties

Figure 11 shows the strength recovery of the control prism (C) and the prisms containing different hydrogels. Since H-c and H-d showed relatively similar reabsorption results, as shown in Fig. 3, H-c was not utilized in the strength recovery and crack closure experiments. It is seen that all hydrogels improved the strength recovery of the prisms compared to the control prism. While the control prism reached a maximum of 34% strength recovery, the prisms containing H-b achieved about 62% of strength recovery, followed by H-a and H-d. The 34% strength recovery of the control prism is comparable with the strength recovery of 40–45% obtained in the previous studies [52, 87, 88]. The observed strength recovery in the control prism is attributed to the intrinsic self-healing ability of the cementitious materials.

At early ages, the healing products are expected to consist more of the continued hydration products of unhydrated cement on the crack surface, while in later ages, the calcium carbonate crystallization will govern the overall healing. It has been reported that at the age of 28 days of healing, the self-healing mechanism is mostly the stitching of the crack by further hydration and calcium carbonate around hydrogels [89]. Macrovoids formed by hydrogels act as crack initiators; in other words, the crack path likely follows the position of the macrovoids. The hydrogels are then available for swelling upon crack formation, as the crack runs through the macrovoids. In the prisms with hydrogels, the water absorbed in hydrogels during the wet periods is slowly released into the surrounding region during the dry periods, thereby allowing further formation of healing products in the cracks. It has been previously reported [87, 88] that in samples without hydrogels and subjected to an environment with a relative humidity of RH = 90% and 60%, very small regain in mechanical loading, 23% and 13%, respectively, was observed. This indicates the importance of supply of water in the healing process.

3.9 Crack filling

The crack filling evolution of the prisms was studied to provide insight into the self-healing mechanisms of the prisms. The crack filling was observed after 1, 3, 7, 14, and 28 cycles of healing. The crack width before healing was examined via optical microscopy in all prisms and measured to be 60 ± 8 μm. As can be seen in Fig. 12, the cracks were filled by formation of white crystal-like materials. The presence of the healing products was observed on both sides of the prisms. It was noted that the control prism without hydrogels showed formation of the healing products after the third cycle. All the prisms containing hydrogels demonstrated complete crack filling at the age of 28 days. However, at this age, the crack in the control sample without hydrogel was only partially filled. A distinct feature in the case of the C H-a is that the entire crack appeared to be healed completely after 7 cycles. Regarding C H-a and C H-d, a noticeable difference in the crack filling behavior of these prisms cannot be inferred from the optical images. One relevant observation is that the crack width is not the same for all samples even though the crack formation procedure

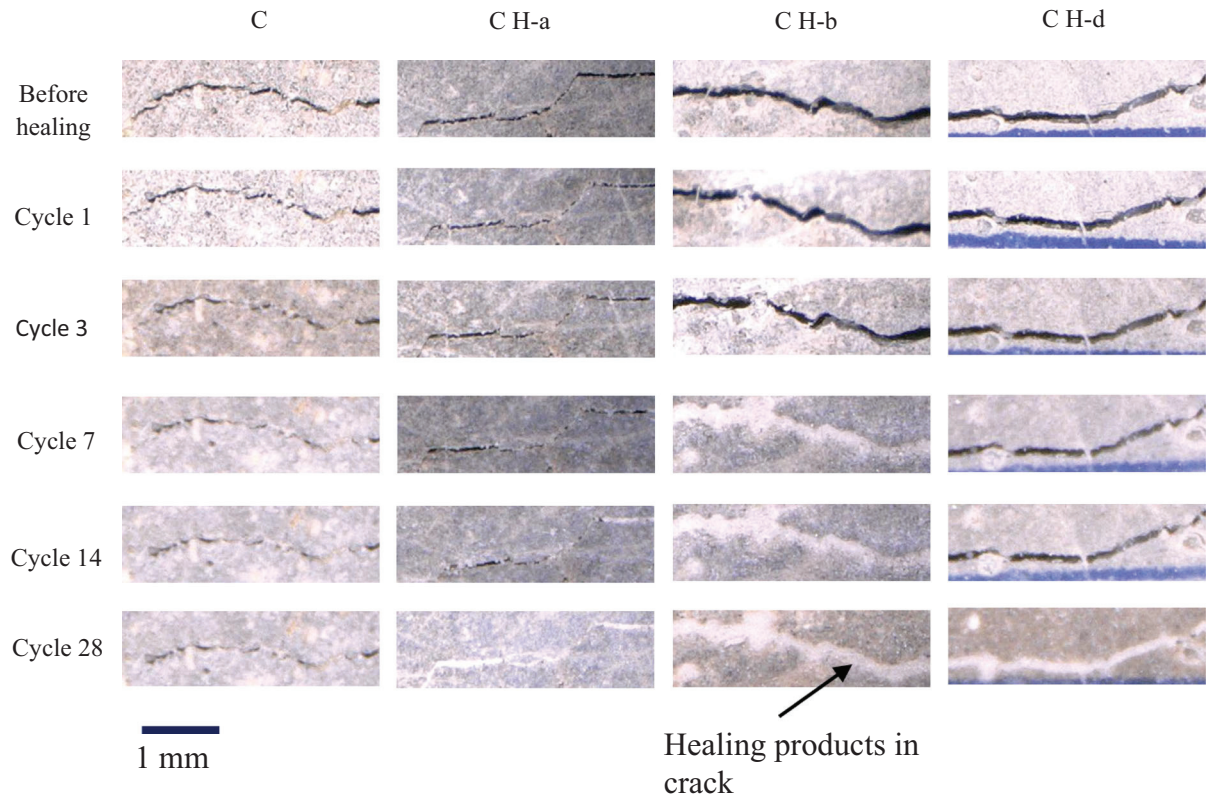

Fig. 12 Optical images showing the crack filling evolution of the control prism and the prisms with different hydrogels. The scale bar is the same for all images

was the same for all samples and the same crack mouth displacement was utilized in all samples. This can potentially affect the crack filling in the samples and hinder us to see the differences in the crack filling ability of these two hydrogels.

An examination of the strength recovery and crack filling results and the sorption of the pastes, as shown in Fig. 4, could help to shed light on the underlying effect of the hydrogels on the self-healing of cement paste. An important observation from the results is that among the hydrogel modified pastes, the strength recovery and crack filling of the pastes seemed to have a relationship with the sorption of the hydrogel-modified pastes, as shown in Fig. 4. Such relationships have not been explored in previous investigations and provide valuable contributions to the state-of-the-art in the self-healing of cementitious materials using hydrogels. It is seen that C H-b demonstrated the highest strength recovery and crack filling compared to C H-a and C H-d; this sample also showed the highest sorption. The difference in the sorption of C H-a and C H-d was small; thus, these two pastes showed similar strength recovery and crack filling. As discussed previously, the presence of water is integral to the chemical reactions involved in the precipitation of the healing products and is needed for the transport of ions from the bulk to the crack surface. In this study, H-b showed the highest absorption and re-absorption and C H-b exhibited the highest sorption. However, such a link was not as clear in the case of other hydrogels. Establishing a robust correlation between the self-healing performance and the characteristics of hydrogels would require including a larger number of different hydrogels in the study, which is currently underway and will be reported in the future contributions.

4 Conclusions

While several prior studies examined the self-healing property of hydrogels in cementitious materials, the

relationship between the characteristics of hydrogels and their self-healing is not well understood. Thus, the novelty of this paper is to explore the dependence of self-healing in cementitious materials on the hydrogel characteristics. Such information is needed for the design of hydrogels and developing guidelines for self-healing applications. The effect of four hydrogels with different absorption properties on the chemical characteristics of the healing products and self-healing of cement pastes was examined. FTIR, TGA, and SEM/EDS indicated that C–S–H, ettringite, CH, and CC were the main phases in the healing products. The combined CC and CH content of the healing products was shown to be noticeably higher than that in the bulk cement pastes. Among hydrogel modified pastes, CC content in the healing products appears to increase with sorption in the pastes. The optical imaging indicated that the crack filling seams to improve with sorption in the pastes. Similarly, the strength recovery of the healed cracked pastes was shown to enhance with sorption of the paste. Thus, our results provide evidence on the relationship between self-healing and sorption in hydrogel modified pastes. It should be noted that other parameters, including mix design and healing condition, affect the healing performance of the materials containing hydrogels and thus, further studies are required to investigate the effect of these parameters.

Acknowledgements This study was supported by the National Science Foundation under the CAREER Award Number 1846984. Any opinions, findings, conclusions, or recommendations expressed in this material are those of the author(s) and do not necessarily reflect the views of the National Science Foundation.

Declarations

Conflict of interest The authors declare that they have no conflict of interest.

References

1. Mignon A, Snoeck D, Schaubroeck D, Luickx N, Dubruel P, van Vlierberghe S, de Belie N (2015) pH-responsive superabsorbent polymers: a pathway to self-healing of mortar. React Funct Polym 93:68–76. https://doi.org/10.1016/j.reactfunctpolym.2015.06.003
2. Xu J, Yao W (2014) Multiscale mechanical quantification of self-healing concrete incorporating non-ureolytic bacteria-based healing agent. Cem Concr Res 64:1–10. https://doi.org/10.1016/j.cemconres.2014.06.003
3. Wang K, Jansen DC, Shah SP, Karr AF (1997) Permeability study of cracked concrete. Cem Concr Res 27:381–393
4. Pacheco-Torgal F, Abdollahnejad Z, Miraldo S, Baklouti S, Ding Y (2012) An overview on the potential of geopolymers for concrete infrastructure rehabilitation. Constr Build Mater 36:1053–1058. https://doi.org/10.1016/j.conbuildmat.2012.07.003
5. Edvardsen C (1999) Water permeability and autogenous healing of cracks in concrete. In: Innovation in concrete structures: design and construction. Thomas Telford Publishing, pp 473–487
6. Schröfl C, Erk KA, Siriwatwechakul W, Wyrzykowski M, Snoeck D (2022) Recent progress in superabsorbent polymers for concrete. Cem Concr Res 151:106648. https://doi.org/10.1016/j.cemconres.2021.106648
7. Wu M, Johannesson B, Geiker M (2012) A review: self-healing in cementitious materials and engineered cementitious composite as a self-healing material. Constr Build Mater 28:571–583. https://doi.org/10.1016/j.conbuildmat.2011.08.086
8. Homma D, Mihashi H, Nishiwaki T (2009) Self-healing capability of fibre reinforced cementitious composites. J Adv Concr Technol 7:217–228
9. Li M, Li VC (2011) Cracking and healing of engineered cementitious composites under chloride environment. ACI Mater J 108:333
10. Neville A (2002) Autogenous healing: a concrete miracle? Concr Int 24:76–82
11. ter Heide N, Schlangen E (2007) Self-healing of early age cracks in concrete. In: First international conference on self healing materials, pp 1–12
12. van Tittelboom K, Wang J, Araújo M, Snoeck D, Gruyaert E, Debbaut B, Derluyn H, Cnudde V, Tsangouri E, van Hemelrijck D, de Belie N (2016) Comparison of different approaches for self-healing concrete in a large-scale lab test. Constr Build Mater 107:125–137. https://doi.org/10.1016/j.conbuildmat.2015.12.186
13. van Tittelboom K, de Belie N (2013) Self-healing in cementitious materials-a review. Materials. https://doi.org/10.3390/ma6062182
14. Snoeck D, de Belie N (2016) Repeated autogenous healing in strain-hardening cementitious composites by using superabsorbent polymers. J Mater Civ Eng 25:864–870. https://doi.org/10.1061/(ASCE)MT.1943-5533
15. Lefever G, Snoeck D, Aggelis DG, de Belie N, van Vlierberghe S, van Hemelrijck D (2020) Evaluation of the self-healing ability of mortar mixtures containing superabsorbent polymers and nanosilica. Materials. https://doi.org/10.3390/ma13020380
16. Schröfl C, Erk KA, Siriwatwechakul W, Wyrzykowski M, Snoeck D (2022) Recent progress in superabsorbent polymers for concrete. Cem Concr Res. https://doi.org/10.1016/j.cemconres.2021.106648
17. Hong G, Song C, Choi S (2020) Autogenous healing of early-age cracks in cementitious materials by superabsorbent polymers. Materials. https://doi.org/10.3390/ma13030690

18. Snoeck D, de Schryver T, de Belie N (2018) Enhanced impact energy absorption in self-healing strain-hardening cementitious materials with superabsorbent polymers. Constr Build Mater 191:13–22. https://doi.org/10.1016/j.conbuildmat.2018.10.015
19. Farzanian K, Vafaei B, Ghahremaninezhad A (2021) The influence of the chemical composition of hydrogels on their behavior in cementitious materials. Mater Struct. https://doi.org/10.1617/s11527-021-01838-z
20. Fořt J, Migas P, Černý R (2020) Effect of absorptivity of superabsorbent polymers on design of cement mortars. Materials 13:1–16. https://doi.org/10.3390/ma13235503
21. Kalinowski M, Woyciechowski P (2021) Chloride diffusion in concrete modified with polyacrylic superabsorbent polymer (Sap) hydrogel—the influence of the water-to-cement ratio and sap-entrained water. Materials. https://doi.org/10.3390/ma14154064
22. Vafaei B, Farzanian K, Ghahremaninezhad A (2021) Effect of hydrogels containing nanosilica on the properties of cement pastes. J Compos Sci 5:105
23. Montanari L, Suraneni P, Weiss WJ (2017) Accounting for water stored in superabsorbent polymers in increasing the degree of hydration and reducing the shrinkage of internally cured cementitious mixtures. Adv Civ Eng Mater 6:583–599
24. Farzanian K, Vafaei B, Ghahremaninezhad A (2019) The behavior of superabsorbent polymers (SAPs) in cement mixtures with glass powders as supplementary cementitious materials. Materials. https://doi.org/10.3390/ma12213597
25. Farzanian K, Ghahremaninezhad A (2018) On the interaction between superabsorbent hydrogels and blended mixtures with supplementary cementitious materials. Adv Civ Eng Mater 7:567–589
26. Bazhuni MF, Kamali M, Ghahremaninezhad A (2019) An investigation into the properties of ternary and binary cement pastes containing glass powder. Front Struct Civ Eng 13:741–750
27. Vafaei B, Farzanian K, Ghahremaninezhad A (2020) The influence of superabsorbent polymer on the properties of alkali-activated slag pastes. Constr Build Mater. https://doi.org/10.1016/j.conbuildmat.2019.117525
28. Jiang D, Li X, Lv Y, Li C, Jiang W, Liu Z, Xu J, Zhou Y, Dan J (2021) Autogenous shrinkage and hydration property of alkali activated slag pastes containing superabsorbent polymer. Cem Concr Res 149:106581. https://doi.org/10.1016/j.cemconres.2021.106581
29. Yang J, Snoeck D, de Belie N, Sun Z (2021) Effect of superabsorbent polymers and expansive additives on the shrinkage of alkali-activated slag. Cem Concr Compos 123:104218. https://doi.org/10.1016/j.cemconcomp.2021.104218
30. Wang P, Chen H, Chen P, Pan J, Xu Y, Wang H, Shen W, Cao K (2020) Effect of internal curing by super absorbent polymer on the autogenous shrinkage of alkali-activated slag mortars. Materials 13:1–13. https://doi.org/10.3390/ma13194318
31. Prabahar J, Vafaei B, Ghahremaninezhad A (2022) The effect of hydrogels with different chemical compositions on the behavior of alkali-activated slag pastes. Gels 8:731. https://doi.org/10.3390/gels8110731
32. Snoeck D, De Belie N (2019) Autogenous healing in strain-hardening cementitious materials with and without superabsorbent polymers: an 8-year study. Front Mater. https://doi.org/10.3389/fmats.2019.00048
33. Snoeck D (2022) Autogenous healing in 10-years aged cementitious composites using microfibers and superabsorbent polymers. Infrastructures (Basel). https://doi.org/10.3390/infrastructures7100129
34. Mignon A, Vermeulen J, Snoeck D, Dubruel P, van Vlierberghe S, de Belie N (2017) Mechanical and self-healing properties of cementitious materials with pH-responsive semi-synthetic superabsorbent polymers. Mater Struct Mater Constr. https://doi.org/10.1617/s11527-017-1109-4
35. Lefever G, van Hemelrijck D, Aggelis DG, Snoeck D (2022) Evaluation of self-healing in cementitious materials with superabsorbent polymers through ultrasonic mapping. Constr Build Mater. https://doi.org/10.1016/j.conbuildmat.2022.128272
36. Snoeck D, Dewanckele J, Cnudde V, de Belie N (2016) X-ray computed microtomography to study autogenous healing of cementitious materials promoted by superabsorbent polymers. Cem Concr Compos 65:83–93. https://doi.org/10.1016/j.cemconcomp.2015.10.016
37. Snoeck D, Pel L, De Belie N (2020) Autogenous healing in cementitious materials with superabsorbent polymers quantified by means of NMR. Sci Rep. https://doi.org/10.1038/s41598-020-57555-0
38. Gruyaert E, Debbaut B, Snoeck D, Díaz P, Arizo A, Tziviloglou E, Schlangen E, De Belie N (2016) Self-healing mortar with pH-sensitive superabsorbent polymers: testing of the sealing efficiency by water flow tests. Smart Mater Struct. https://doi.org/10.1088/0964-1726/25/8/084007
39. Wang JY, Soens H, Verstraete W, de Belie N (2014) Self-healing concrete by use of microencapsulated bacterial spores. Cem Concr Res 56:139–152. https://doi.org/10.1016/j.cemconres.2013.11.009
40. Baffoe E, Ghahremaninezhad A (2022) On the interaction between proteins and cracked cementitious surface. Constr Build Mater 352:128982. https://doi.org/10.1016/j.conbuildmat.2022.128982
41. Baffoe E, Ghahremaninezhad A (2022) The effect of biomolecules on enzyme-induced calcium carbonate precipitation in cementitious materials. Constr Build Mater 345:128323. https://doi.org/10.1016/j.conbuildmat.2022.128323
42. Snoeck D, van Tittelboom K, Steuperaert S, Dubruel P, de Belie N (2014) Self-healing cementitious materials by the combination of microfibres and superabsorbent polymers. J Intell Mater Syst Struct 25:13–24. https://doi.org/10.1177/1045389X12438623
43. Chindasiriphan P, Yokota H, Pimpakan P (2020) Effect of fly ash and superabsorbent polymer on concrete self-healing ability. Constr Build Mater 233:116975. https://doi.org/10.1016/j.conbuildmat.2019.116975
44. Lefever G, Aggelis DG, de Belie N, Raes M, Hauffman T, van Hemelrijck D, Snoeck D (2020) The influence of superabsorbent polymers and nanosilica on the hydration process and microstructure of cementitious mixtures. Materials 13:1–16. https://doi.org/10.3390/ma13225194
45. Krafcik MJ, Erk KA (2016) Characterization of superabsorbent poly (sodium-acrylate acrylamide) hydrogels and

influence of chemical structure on internally cured mortar. Mater Struct 49:4765–4778. https://doi.org/10.1617/s11527-016-0823-7
46. Krafcik MJ, Bose B, Erk KA (2018) Synthesis and characterization of polymer-silica composite hydrogel particles and influence of hydrogel composition on cement paste microstructure. Adv Civ Eng Mater 7:590–613. https://doi.org/10.1520/ACEM20170144
47. Zhu Q, Barney CW, Erk KA (2015) Effect of ionic crosslinking on the swelling and mechanical response of model superabsorbent polymer hydrogels for internally cured concrete. Mater Struct 48:2261–2276. https://doi.org/10.1617/s11527-014-0308-5
48. Krafcik MJ, Macke ND, Erk KA (2017) Improved concrete materials with hydrogel-based internal curing agents. Gels 3:46. https://doi.org/10.3390/gels3040046
49. Farzanian K, Ghahremaninezhad A (2018) Desorption of superabsorbent hydrogels with varied chemical compositions in cementitious materials. Mater Struct Mater Constr. https://doi.org/10.1617/s11527-017-1128-1
50. Farzanian K, Ghahremaninezhad A (2018) On the effect of chemical composition on the desorption of superabsorbent hydrogels in contact with a porous cementitious material. Gels 4:70. https://doi.org/10.1617/s11527-017-1068-9
51. Snoeck D, Steuperaert S, van Tittelboom K, Dubruel P, de Belie N (2012) Visualization of water penetration in cementitious materials with superabsorbent polymers by means of neutron radiography. Cem Concr Res 42:1113–1121
52. Snoeck D (2016) Self-healing and microstructure of cementitious materials with microfibres and superabsorbent polymers. http://studwww.ugent.be/~dsnoeck/PhD/PhDDidierSnoeck.pdf
53. Snoeck D, van den Heede P, van Mullem T, de Belie N (2018) Water penetration through cracks in self-healing cementitious materials with superabsorbent polymers studied by neutron radiography. Cem Concr Res 113:86–98. https://doi.org/10.1016/j.cemconres.2018.07.002
54. Prabahar J, Vafaei B, Baffoe E, Ghahremaninezhad A (2022) The effect of biochar on the properties of alkali-activated slag pastes. Constr Mater 2:1–14
55. Snoeck D, Schröfl C, Mechtcherine V (2018) Recommendation of RILEM TC 260-RSC: testing sorption by superabsorbent polymers (SAP) prior to implementation in cement-based materials. Mater Struct Mater Constr. https://doi.org/10.1617/s11527-018-1242-8
56. Huang H, Ye G, Damidot D (2013) Characterization and quantification of self-healing behaviors of microcracks due to further hydration in cement paste. Cem Concr Res 52:71–81. https://doi.org/10.1016/j.cemconres.2013.05.003
57. Mignon A, Graulus GJ, Snoeck D, Martins J, de Belie N, Dubruel P, van Vlierberghe S (2014) pH-sensitive superabsorbent polymers: a potential candidate material for self-healing concrete. J Mater Sci 50:970–979. https://doi.org/10.1007/s10853-014-8657-6
58. Schröfl C, Mechtcherine V, Gorges M (2012) Relation between the molecular structure and the efficiency of superabsorbent polymers (SAP) as concrete admixture to mitigate autogenous shrinkage. Cem Concr Res 42:865–873. https://doi.org/10.1016/j.cemconres.2012.03.011
59. Boshoff W, Mechtcherine V, Snoeck D, Schröfl C, De Belie N, Ribeiro AB, Cusson D, Wyrzykowski M, Toropovs N, Lura P (2020) The effect of superabsorbent polymers on the mitigation of plastic shrinkage cracking of conventional concrete, results of an inter-laboratory test by RILEM TC 260-RSC. Mater Struct Mater Constr. https://doi.org/10.1617/s11527-020-01516-6
60. Kim YY, Lee KM, Bang JW, Kwon SJ (2014) Effect of W/C ratio on durability and porosity in cement mortar with constant cement amount. Adv Mater Sci Eng. https://doi.org/10.1155/2014/273460
61. Lothenbach B, Le Saout G, Ben Haha M, Figi R, Wieland E (2012) Hydration of a low-alkali CEM III/B–SiO_2 cement (LAC). Cem Concr Res 42:410–423
62. Esteves LP (2011) On the hydration of water-entrained cement-silica systems: combined SEM, XRD and thermal analysis in cement pastes. Thermochim Acta 518:27–35. https://doi.org/10.1016/J.TCA.2011.02.003
63. Hall C, Barnes P, Billimore AD, Jupe AC, Turrillas X (1996) Thermal decomposition of ettringite $Ca_6[Al(OH)_6]_2(SO_4)_3{\cdot}26H_2O$. J Chem Soc Faraday Trans 92:2125–2129. https://doi.org/10.1039/FT9969202125
64. Snoeck D, Jensen OM, de Belie N (2015) The influence of superabsorbent polymers on the autogenous shrinkage properties of cement pastes with supplementary cementitious materials. Cem Concr Res 74:59–67. https://doi.org/10.1016/j.cemconres.2015.03.020
65. Kamali M, Ghahremaninezhad A (2017) An investigation into the influence of superabsorbent polymers on the properties of glass powder modified cement pastes. Constr Build Mater 149:236–247. https://doi.org/10.1016/j.conbuildmat.2017.04.125
66. Esteves LP (2011) On the hydration of water-entrained cement–silica systems: combined SEM, XRD and thermal analysis in cement pastes. Thermochim Acta 518:27–35
67. Ye G, Liu X, de Schutter G, Poppe A-M, Taerwe L (2007) Influence of limestone powder used as filler in SCC on hydration and microstructure of cement pastes. Cem Concr Compos 29:94–102
68. Pane I, Hansen W (2005) Investigation of blended cement hydration by isothermal calorimetry and thermal analysis. Cem Concr Res 35:1155–1164
69. Tobón JI, Payá JJ, Borrachero M, Restrepo OJ (2012) Mineralogical evolution of Portland cement blended with silica nanoparticles and its effect on mechanical strength. Constr Build Mater 36:736–742
70. Senff L, Labrincha JA, Ferreira VM, Hotza D, Repette WL (2009) Effect of nano-silica on rheology and fresh properties of cement pastes and mortars. Constr Build Mater 23:2487–2491. https://doi.org/10.1016/j.conbuildmat.2009.02.005
71. Wu L, Zhang Z, Yang M, Yuan J, Li P, Men X (2020) Graphene enhanced and in situ-formed alginate hydrogels for reducing friction and wear of polymers. Colloids Surf A Physicochem Eng Asp. https://doi.org/10.1016/j.colsurfa.2020.124434
72. Ashraf M, Khan AN, Ali Q, Mirza J, Goyal A, Anwar AM (2009) Physico-chemical, morphological and thermal analysis for the combined pozzolanic activities of minerals additives. Constr Build Mater 23:2207–2213

73. Thongsanitgarn P, Wongkeo W, Chaipanich A (2014) Hydration and compressive strength of blended cement containing fly ash and limestone as cement replacement. J Mater Civ Eng 26:2–6. https://doi.org/10.1061/(ASCE)MT.1943-5533.0001002
74. Mitchell L, Margeson J (2006) The effects of solvents on C-S–H as determined by thermal analysis. J Therm Anal Calorim 86:591–594
75. Dent Glasser LS, Lachowski EE, Mohan K, Taylor HFW (1978) A multi-method study of C_3S hydration. Pergamon Press, Oxford
76. Taylor HFW (1997) Cement chemistry. Thomas Telford, London
77. Mills R, Lobo VMM (1989) Self-diffusion in electrolyte solutions. Physical sciences data, vol 36. Elsevier, Amsterdam
78. Wu L, Farzadnia N, Shi C, Zhang Z, Wang H (2017) Autogenous shrinkage of high performance concrete: a review. Constr Build Mater 149:62–75. https://doi.org/10.1016/j.conbuildmat.2017.05.064
79. Yu P, Kirkpatrick RJ, Poe B, McMillan PF, Cong X (1999) Structure of calcium silicate hydrate (C–S–H): near-, mid-, and far-infrared spectroscopy. J Am Ceram Soc 82:742–748
80. Yılmaz B, Olgun A (2008) Studies on cement and mortar containing low-calcium fly ash, limestone, and dolomitic limestone. Cem Concr Compos 30:194–201
81. Kamali M, Ghahremaninezhad A (2018) Effect of biomolecules on the nanostructure and nanomechanical property of calcium-silicate-hydrate. Sci Rep 8:1–16. https://doi.org/10.1038/s41598-018-27746-x
82. Kamali M, Ghahremaninezhad A (2018) A study of calcium-silicate-hydrate/polymer nanocomposites fabricated using the layer-by-layer method. Materials 11:527. https://doi.org/10.3390/ma11040527
83. Vladu CM, Hall C, Maitland GC (2006) Flow properties of freshly prepared ettringite suspensions in water at 25 °C. J Colloid Interface Sci 294:466–472
84. Mondal P, Shah S, Marks L (2008) Nanoscale characterization of cementitious materials. ACI Mater J 105:174–179
85. Dijkstra H (1998) EDXA operater's school course manual
86. Glasser LSD, Lachowski EE, Mohan K, Taylor HFW (1978) A multi-method study of C3S hydration. Cem Concr Res 8:733–739
87. Yang E-H (2008) Designing added functions in engineered cementitious composites
88. Yang Y, Lepech MD, Yang E-H, Li VC (2009) Autogenous healing of engineered cementitious composites under wet–dry cycles. Cem Concr Res 39:382–390
89. Snoeck D (2015) Self-healing and microstructure of cementitious materials with microfibres and superabsorbent polymers